Journal of Sound and Vibration 329 (2010) 5289–5306

Contents lists available at ScienceDirect

Journal of Sound and Vibration

journal homepage: www.elsevier.com/locate/jsvi

Dynamics behavior of rotating bladed discs: A finite element formulation for the study of second and higher order harmonics

Giancarlo Genta [a], Chen Feng [b,*], Andrea Tonoli [b]

[a] Mechanics Department, Politecnico di Torino, 10129 Torino, Italy
[b] Mechanics Department, Mechatronics Laboratory, Politecnico di Torino, Italy

ARTICLE INFO

Article history:
Received 15 April 2010
Received in revised form
13 July 2010
Accepted 14 July 2010
Handling Editor: H. Ouyang
Available online 29 July 2010

ABSTRACT

Annular finite elements for the computation of second and higher order harmonics modes of bladed rotating discs are developed. The elements take into account gyroscopic effect and stiffening due to centrifugal and thermal stresses (the latter not present in arrays of blades). The displacement field is expressed by a truncated Fourier series along the angle and by polynomial shape functions in the radial direction. This paper is the generalization of a previous study limited to zero- and first-order harmonics and deals only with second and higher order harmonics modes that are uncoupled from the modes involving the behavior of the rotor as a whole. Several cases have been studied to verify the accuracy of the disc and array of blades elements.

1. Introduction

Many rotors, like those of turbomachinery, can be modeled as composed of shafts, discs and arrays of blades. In elementary rotordynamics, the bladed discs are assumed to be rigid bodies, contributing to the inertia of the rotor but not to its compliance. However, there are cases like, for instance, circular saws [1] and some turbomachines [2–5], in which the deformation of the discs and possibly of the blades must be accounted for since the rigid body assumption does not allow a detailed dynamic analysis. Sometimes, the dynamic behavior of the blades influences the whole system [6], possibly giving way to dangerous phenomena, such as instability [7]. When the compliance of the discs is important, centrifugal and thermo-elastic loading due to temperature gradients can affect the dynamic behavior and must be taken into account. The dynamics of a bladed disc can be studied without any problem by using any commercial FEM code if no account is taken for its rotation, but things become more complex when gyroscopic and centrifugal stiffening effects due to rotation must be considered. The latter effect can be accounted for by using the geometric stiffness matrix as in [2,3,8] for discs and in [6,9] for arrays of blades. An effect similar to centrifugal stiffness can be due to temperature gradients: it can be accounted for using the geometric matrix as well [8]. Choi and Lee [10] have also studied the transient thermo-elastic behavior of discs, obtaining a useful tool to improve the performance of the discs.

The blades can be modeled as an array of beams attached to the outer edge of the disc and this has been successfully done for studying the interaction between discs and blades, but this approach does not allowed to predict the local modes of the blades [11]. Genta and Tonoli [9] developed a model of coupled disc-blade assemblies which includes Coriolis effects due to rotation but the modes related to second and higher order harmonics of the array of blades have still been neglected.

* Corresponding author.
E-mail addresses: giancarlo.genta@polito.it (G. Genta), feng.chen@polito.it (C. Feng), andrea.tonoli@polito.it (A. Tonoli).
URLS: http://www.giancarlogenta.it (G. Genta), http://www.lim.polito.it (A. Tonoli).

0022-460X/$ - see front matter © 2010 Elsevier Ltd. All rights reserved.
doi:10.1016/j.jsv.2010.07.015

Nomenclature

$A(r)$	blade section area at radius r
A,B,C,D	shape function components
C	original coordinate
D	disc element elastic properties
E	Young's modulus
$F_{r,i}$	centrifugal force of each blade
G	gyroscopic matrix
$h(r)$	thickness of disc at radius r
I_v, I_w	section area moment of inertia
k	elastic stiffness matrices
K	elastic stiffness matrix
m	mass matrices
M	mass matrix
n	number of harmonic terms
$\mathbf{n}_u(\chi)$	radial shape functions
$\mathbf{n}_v(\chi)$	tangential shape functions
$\mathbf{n}_w(\chi)$	axial shape functions
N	number of blades
P	coordinate vector of point P
$P_{r\omega}$	radial force per unit ω
q	element d.o.f.
Q	element complex d.o.f.
r_i,r_0	inner and outer radius
$\mathbf{R}_k$	rotation matrices
T_i	kinetic energy
U_i	potential energy
$\boldsymbol{\varepsilon}_i$	generalized strain vector
θ	angular location in disc
v	Poisson's ratio
ρ	element density
σ	element stress
χ	non-dimensional radius
ω	spin speed of the shaft
ψ	pretwist angle of the blade

Subscripts

c	circumferential
e	elastic component
g	geometric component
i	i th-order harmonic component
ic, is	i th-order harmonic functions
inp,i	in-plane components
j,i	i th-order harmonic of jth blade
outp,i	out-of-plane components
r	radial
T	due to temperature gradient
uu, uv, vv,ww	in-plane and out-of-plane
ω	due to rotation speed

Chun and Lee [12] demonstrated that the stagger angle of the blades determines an inertial coupling between the in-plane and out-of-plane of the disc motion and that only the zero and one nodal diameter are coupled to the dynamics of the shaft. Genta and Tonoli [8,9] use a complex coordinates approach to derive the equation of motion of disc and array of blades finite elements that takes into account the blades' stagger angle, but considered only the modes of the disc that are coupled with those of the rotor as a whole and neglected second and higher order harmonics.

Tomioka et al. [13] model the connection between flexible discs and arrays of blades by introducing a spring element at the interface, while Genta and Tonoli [9] use a disc-array of blades transition element to model the connection. They introduce also a shaft–disc transition element to describe the interface between the shaft and the discs [8].

Ruzicka and Hodges [14] demonstrate that shortcomings exist when performing modal reduction for rotor blades using classical, displacement-based finite elements and that mixed finite element should be instead in such procedure.

Dynamic instability of rotating discs in contact with stationary pads have been shown for circular saws and for disc brakes; the latter case is studied using the finite element method by Kang [15] taking into account both gyroscopic and centrifugal stiffening effect. It is highlighted that the friction coefficient has an important role in the in-plane torsional vibration of the disc.

Lim [16] introduces a harmonic disc element for the case of disk drive spindle systems to study the flexural vibrations and coupling between the shaft and disc. Structural flexibility is taken into account for each component, but the centrifugal effect is only considered in the discs. Such finite element models are assembled and applied to the case of HDDs and the effectiveness and accuracy of the proposed approach is verified.

It is important to study the higher order modes of the disc and array of blades even if they are not coupled to the shaft dynamics since they can be excited at a resonance and compromise the safety of the rotor system. The aim of the present paper is to generalize the finite element formulation taking into account both the gyroscopic effect and centrifugal stiffening to study the flexural behavior in the flexible discs and array of blades which have already been introduced in [8,9] to include also disc and blades modes that are uncoupled with the rotor modes.

The basic approach is what usually defined as $1\frac{1}{2}$ dimensional approach, i.e. the shaft is modeled as a beam (one-dimensional solid) and the discs and the arrays of blades are assumed to be annular elements with displacements developed in Fourier series along the angle.

The discs are connected to the shaft and a shaft–disc transition element is used as interface, while blades are assumed to be attached to the outer diameter of the discs and the interface is simulated by a disc–array of blades transition element. The element matrices are developed by a Lagrange approach and written in the complex coordinate described in Refs. [17,18]. The element matrices are programmed in the existing FEM code DYNROT [19]. The model is validated in different cases comparing its results with analytical ones taken from the literature and numerical simulations performed using

commercial codes. The accuracy of the dynamic behavior of the second and higher order harmonics disc and array of blades elements have been checked.

2. Second and higher order harmonics disc element

2.1. Element kinematics

The element is modeled as a two-dimensional annular object, with all properties concentrated at its mid-plane. In addition, it is assumed to be perfectly balanced, i.e. its center of mass lies in its geometrical center and its principal axis of inertia coincides with its rotation axis. However, a static and couple unbalance can be added into the equations of motion later.

The deformation of the bladed disc is made by a rigid body configuration deviation and a compliant body deformation. During the deformation, the mid-plane of the disc is assumed to maintain the same orientation in space of a rigid body attached to the relevant shaft cross-section, while the disc exits its mid-plane owing to its flexibility.

The generalized coordinates can be defined with reference to the frames shown in Fig. 1. Frame *OXYZ* is the inertial frame with the origin at *O* and *Z*-axis coinciding with the rotor rotation axis in its undeformed position; frame Ox^*y^*Z is the rotating frame, axes x^* and y^* rotate in the *XY*-plane at a rotating speed ω (at constant speed condition it is rotated by angle ωt); frame $CX'Y'Z'$ has its original point *C* located at the center of the shaft in the disc attachment cross-section, but its axes remain parallel to axes *X*,*Y*,*Z*. The deformed position of a generic point *P* on the disc can be defined by the following rotations:

Rotate the axes of $CX'Y'Z'$ frame about the X'-axis by an angle Φ_x until Y'-axis enters the mid-plane of the disc in its deformed configuration; let the axes so obtained be y_x and z_x and the rotation matrix expressing the coordinates of *P* in $CX'Y'Z'$ frame from those referred to $CX'y_xz_x$ be $\mathbf{R}_1$.

Rotate frame $CX'y_xz_x$ about y_x-axis by an angle Φ_y until X'-axis enters the mid-plane of the disc in its deformed configuration; let the axes so obtained be x_y and z_y and the rotation matrix be $\mathbf{R}_2$.

Rotate frame $Cx_yy_xz_y$ in x_yy_x plane through an angle $\Phi_z+\omega t$, define the so-obtained frame as *Cxyz*, which is fixed to the mid-plane of the disc and will be referred to as the rotating and whirling frame, and the rotation matrix refer to the rotating about *z*-axis can be split into two terms $\mathbf{R}_3$ (rotation Φ_z) and $\mathbf{R}_4$ (rotation ωt). The expressions for the above-mentioned rotating matrices are defined in Refs. [8,18].

Let u, v and w be, respectively, the radial, tangential and axial displacement components of a generic point whose undeformed position P_0 is defined by radius r and angle θ in the reference frame *Cxyz* defined above that follows both the rotation and the deformation of the shaft. The position of point *P* after deformation is

$$(\overline{\mathbf{P}-\mathbf{O}}) = (\overline{\mathbf{C}-\mathbf{O}}) + \prod_{k=1}^{4} \mathbf{R}_k(\{r\ \ 0\ \ z\}^{\mathrm{T}} + \{u\ \ v\ \ w\}^{\mathrm{T}}), \tag{1}$$

where $\mathbf{R}_k$ are rotation matrices mentioned above and they are functions of the angles characterizing the rigid body displacement and of the rotation ωt.

For second and higher order harmonics, the displacement field is uncoupled with the flexural behavior of the rotor and thus rigid body motions need not be included in the formulation. Consequently, the deformation of point P in the inertial reference OXYZ (shown in Fig. 2) related to the *i* th-order harmonics can be expressed by neglecting the displacement $(\overline{\mathbf{C}-\mathbf{O}})$ in Eq. (1).

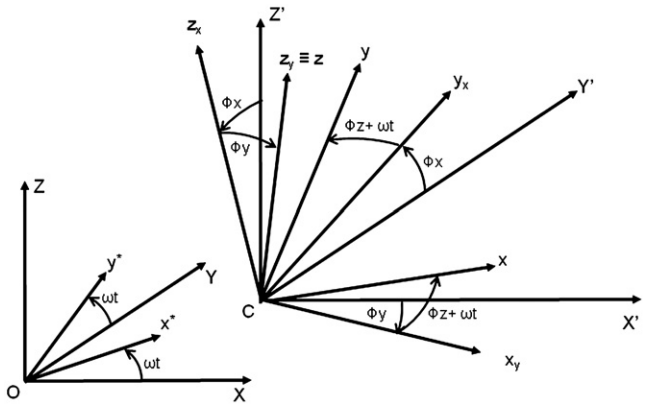

Fig. 1. Reference frames of rotor.

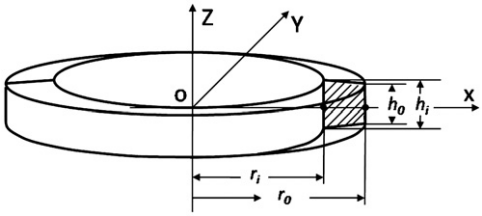

Fig. 2. Sketch of the disc element; r_i, r_0: inner and outer radius of annular disc element; h_i, h_0: thickness of the annular disc element at inner and outer radius.

2.2. Disc element shape functions

An annular finite element with a thickness varying linearly with the radius is shown in Fig. 2. A non-dimensional radial coordinate χ that goes from 0 at the inner radius to 1 at the outer one is defined. The thickness $h(r)$ and the non-dimensional radius χ are thus defined as

$$\chi=(r-r_i)/\Delta r, \quad h=h_i+\chi\Delta h. \tag{2}$$

The displacement field within the element can be expressed as a trigonometrical series in the angular position θ:

$$u(\chi,\theta,z,t)=u_0+\sum_{i=1}^{n}(u_{ic}\cos i\theta+u_{is}\sin i\theta),$$

$$v(\chi,\theta,z,t)=v_0+\sum_{i=1}^{n}(v_{ic}\cos i\theta+v_{is}\sin i\theta),$$

$$w(\chi,\theta,z,t)=w_0+\sum_{i=1}^{n}(w_{ic}\cos i\theta+w_{is}\sin i\theta), \tag{3}$$

where n is the number of harmonic terms. The coefficients of the harmonic terms contributing to the in-plane displacement are u_{ic}, u_{is}, v_{ic} and v_{is}, while those contributing to the out-of-plane displacement are w_{ic} and w_{is}.

It is already noted the dynamic behavior of the zero- and first-order harmonics was studied in Ref. [8]. This paper is focused only on the second and higher order harmonics which are uncoupled from flexural, axial and torsional behavior of the rotor. Furthermore, the orthogonality of the harmonic contributions of the Fourier series expansions of Eq. (3) implies a decoupling between each harmonic. The displacement field of each harmonic can thus be expressed as

$$\begin{cases} u_i(\chi,\theta,t)=u_{ic}\cos i\theta+u_{is}\sin i\theta \\ v_i(\chi,\theta,t)=v_{ic}\cos i\theta+v_{is}\sin i\theta \\ w_i(\chi,\theta,t)=w_{ic}\cos i\theta+w_{is}\sin i\theta \end{cases} \quad \text{for } i\geq 2. \tag{4}$$

As usual in the circular plate's theory, the coefficients of the harmonic terms are functions both of the non-dimensional radius and of time

$$\begin{matrix} u_{ic}(\chi,t), & u_{is}(\chi,t), & v_{ic}(\chi,t) \\ v_{is}(\chi,t), & w_{is}(\chi,t), & w_{ic}(\chi,t) \end{matrix} \quad \text{for } i\geq 2. \tag{5}$$

As usual in the FEM, the matrices of the shape functions are introduced, and the dependence of the displacements on the radius and the time can be expressed as

$$u_{ic}(\chi,t)=\mathbf{n}_u(\chi)\mathbf{q}_{ux}(t), \quad u_{is}(\chi,t)=\mathbf{n}_u(\chi)\mathbf{q}_{uy}(t),$$

$$v_{ic}(\chi,t)=\mathbf{n}_v(\chi)\mathbf{q}_{vx}(t), \quad v_{is}(\chi,t)=\mathbf{n}_v(\chi)\mathbf{q}_{vy}(t),$$

$$w_{ic}(\chi,t)=\mathbf{n}_w(\chi)\mathbf{q}_{wx}(t), \quad w_{is}(\chi,t)=\mathbf{n}_w(\chi)\mathbf{q}_{wy}(t). \tag{6}$$

The shape functions for the in-plane displacements u and v are assumed to be linear; while cubic ones are adopted for the out-of plane displacement w. In terms of the non-dimensional coordinate χ they are

$$\mathbf{n}_u(\chi)=\mathbf{n}_v(\chi)=[1-\chi \;\; \chi], \quad \mathbf{n}_w(\chi)=[Ar_i \;\; B\Delta r \;\; Cr_0 \;\; D\Delta r], \tag{7}$$

where

$$A=2\chi^3-3\chi^2+1, \quad C=2\chi^3-3\chi^2,$$

$$B=-\chi^3+2\chi^2-\chi, \quad D=-\chi^3+\chi^2, \tag{8}$$

where A,B,C,D are shape functions similar to those used in the "simple Timoshenko beam" as reported in Ref. [8].

The generalized coordinates used to express the deformation of the disc deflection field are thus

$$\mathbf{q}_{ux}=\{u_{x1}\ \ u_{x2}\}^{\mathrm{T}},\quad \mathbf{q}_{uy}=\{u_{y1}\ \ u_{y2}\}^{\mathrm{T}},$$

$$\mathbf{q}_{vx}=-\{v_{x1}\ \ v_{x2}\}^{\mathrm{T}},\quad \mathbf{q}_{vy}=\{v_{y1}\ \ v_{y2}\}^{\mathrm{T}},$$

$$\mathbf{q}_{wx}=\{\varphi_{y1}\ \ \beta_{vy1}\ \ \varphi_{y2}\ \ \beta_{vy2}\}^{\mathrm{T}},\quad \mathbf{q}_{wy}=-\{\varphi_{x1}\ \ \beta_{vx1}\ \ \varphi_{x2}\ \ \beta_{vx2}\}^{\mathrm{T}}. \tag{9}$$

Angles φ_{ij} and β_{ij} are defined in Ref. [8].

Two nodes are defined on each disc element when dealing with second and higher order harmonics: nodes 1 and 2, which are located at the inner and the outer radius of the element, respectively. The total number of the real degrees of freedom of the element is 16; nodes 1 and 2 have 8 each. If complex coordinates are introduced into the equations of motion, 8 complex flexural degrees of freedom will result.

2.3. Equations of motion of the element

The generalized coordinates used to approximate the displacements of nodes 1 and 2 describe the deflections of the element from its rigid configurations. The equations of motion of the element are obtained from the expressions of the kinetic and the potential energies and following a Lagrangian approach.

2.3.1. Kinetic energy

The kinetic energy is computed by neglecting the terms related to the deviation of the rigid configurations under the assumption that the thickness of the disc is small compared to the radial dimensions and the shear deformation is negligible.

$\mathbf{P}_i$ denotes the displacement of a point in the mid-plane (z=0) of the element relative to the initial reference frame, the kinetic energy can be written as

$$T_i=\frac{1}{2}\int_{r_i}^{r_0}\int_{-h/2}^{h/2}\int_0^{2\pi}\rho\dot{\mathbf{P}}_i^{\mathrm{T}}\dot{\mathbf{P}}_i r\,\mathrm{d}r\,\mathrm{d}z\,\mathrm{d}\theta, \tag{10}$$

where ρ is the density of the material of the disc element.

The harmonic terms are composed of two uncoupled parts, the in-plane displacement u, v and the out-of-plane term w. So the kinetic energy splits into two independent contributions:

$$T_i=T_{\mathrm{inp},i}+T_{\mathrm{outp},i}. \tag{11}$$

The in-plane and out-of plane contributions to the kinetic energy can be expressed as equations of the shape function and element degrees of freedom, respectively, as

$$\begin{aligned}T_{\mathrm{inp},i}=\tfrac{1}{2}[&\omega^2(\mathbf{q}_{ux}^{\mathrm{T}}\mathbf{m}_{\mathrm{inp},i}\mathbf{q}_{ux}+\mathbf{q}_{uy}^{\mathrm{T}}\mathbf{m}_{\mathrm{inp},i}\mathbf{q}_{uy}+\mathbf{q}_{vx}^{\mathrm{T}}\mathbf{m}_{\mathrm{inp},i}\mathbf{q}_{vx}+\mathbf{q}_{vy}^{\mathrm{T}}\mathbf{m}_{\mathrm{inp},i}\mathbf{q}_{vy}\\&-2\mathbf{q}_{ux}^{\mathrm{T}}\mathbf{m}_{\mathrm{inp},i}\mathbf{q}_{vx}-2\mathbf{q}_{uy}^{\mathrm{T}}\mathbf{m}_{\mathrm{inp},i}\mathbf{q}_{vy})+2\omega(\mathbf{q}_{uy}^{\mathrm{T}}\mathbf{m}_{\mathrm{inp},i}\dot{\mathbf{q}}_{ux}-\mathbf{q}_{vy}^{\mathrm{T}}\mathbf{m}_{\mathrm{inp},i}\dot{\mathbf{q}}_{ux}\\&-\mathbf{q}_{ux}^{\mathrm{T}}\mathbf{m}_{\mathrm{inp},i}\dot{\mathbf{q}}_{uy}+\mathbf{q}_{vx}^{\mathrm{T}}\mathbf{m}_{\mathrm{inp},i}\dot{\mathbf{q}}_{uy}-\mathbf{q}_{uy}^{\mathrm{T}}\mathbf{m}_{\mathrm{inp},i}\dot{\mathbf{q}}_{vx}+\mathbf{q}_{vy}^{\mathrm{T}}\mathbf{m}_{\mathrm{inp},i}\dot{\mathbf{q}}_{vx}+\mathbf{q}_{ux}^{\mathrm{T}}\mathbf{m}_{\mathrm{inp},i}\dot{\mathbf{q}}_{vy}\\&-\mathbf{q}_{vx}^{\mathrm{T}}\mathbf{m}_{\mathrm{inp},i}\dot{\mathbf{q}}_{vy})+\dot{\mathbf{q}}_{ux}^{\mathrm{T}}\mathbf{m}_{\mathrm{inp},i}\dot{\mathbf{q}}_{ux}+\dot{\mathbf{q}}_{uy}^{\mathrm{T}}\mathbf{m}_{\mathrm{inp},i}\dot{\mathbf{q}}_{uy}+\dot{\mathbf{q}}_{vx}^{\mathrm{T}}\mathbf{m}_{\mathrm{inp},i}\dot{\mathbf{q}}_{vx}+\dot{\mathbf{q}}_{vy}^{\mathrm{T}}\mathbf{m}_{\mathrm{inp},i}\dot{\mathbf{q}}_{vy}],\\T_{\mathrm{outp},i}=\tfrac{1}{2}[&\omega^2(\mathbf{q}_{wx}^{\mathrm{T}}\mathbf{m}_{\mathrm{outp},i}\mathbf{q}_{wx}+\mathbf{q}_{wy}^{\mathrm{T}}\mathbf{m}_{\mathrm{outp},i}\mathbf{q}_{wy})+\omega(2\mathbf{q}_{wy}^{\mathrm{T}}\mathbf{m}_{\mathrm{outp},i}\dot{\mathbf{q}}_{wx}-2\mathbf{q}_{wx}^{\mathrm{T}}\mathbf{m}_{\mathrm{outp},i}\dot{\mathbf{q}}_{wy})\\&+\dot{\mathbf{q}}_{wx}^{\mathrm{T}}\mathbf{m}_{\mathrm{outp},i}\dot{\mathbf{q}}_{wx}+\dot{\mathbf{q}}_{wy}^{\mathrm{T}}\mathbf{m}_{\mathrm{outp},i}\dot{\mathbf{q}}_{wy}].\end{aligned} \tag{12}$$

Matrices $\mathbf{m}_{\mathrm{inp},i}$ and $\mathbf{m}_{\mathrm{outp},i}$ are given by the integrals:

$$\mathbf{m}_{\mathrm{inp},i}=2\pi\int_{r_i}^{r_0}\rho r h\mathbf{n}_u^{\mathrm{T}}\mathbf{n}_u\,\mathrm{d}r=2\pi\int_{r_i}^{r_0}\rho r h\mathbf{n}_v^{\mathrm{T}}\mathbf{n}_v\,\mathrm{d}r,$$

$$\mathbf{m}_{\mathrm{outp},i}=\pi\int_{r_i}^{r_0}\rho r h\mathbf{n}_w^{\mathrm{T}}\mathbf{n}_w\,\mathrm{d}r. \tag{13}$$

2.3.2. Potential energy

Contributions to the potential energy due both to the elastic stresses in the material ($U_{e,i}$) and to the 'geometric effect' ($U_{g,i}$) have been considered, as explained in Ref. [8]:

$$U_e=U_{e,i}+U_{g,i}. \tag{14}$$

If the thickness of the disc is small, it can be considered as a rotating Kirchhoff plate and transverse shear deformations can be neglected. The expression of elastic energy of i th-order harmonics due to bending is

$$U_{e,i}=\frac{1}{2}\int_{r_i}^{r_0}\int_0^{2\pi}\boldsymbol{\varepsilon}_i^{\mathrm{T}}\mathbf{D}\boldsymbol{\varepsilon}_i r\,\mathrm{d}r\,\mathrm{d}\theta=U_{e\mathrm{inp},i}+U_{e\mathrm{outp},i}. \tag{15}$$

The generalized strain vector is obtained from the displacement field within the disc; it can be split into the two contributions due to in-plane and out-of-plane deformation

$$\boldsymbol{\varepsilon}_i = \begin{Bmatrix} \boldsymbol{\varepsilon}_{\mathrm{inp},i} \\ \boldsymbol{\varepsilon}_{\mathrm{outp},i} \end{Bmatrix}, \tag{16}$$

where

$$\boldsymbol{\varepsilon}_{\mathrm{inp},i} = \begin{Bmatrix} \dfrac{\partial u_i}{\partial r} \\ \dfrac{u_i}{r} + \dfrac{1}{r}\dfrac{\partial v_i}{\partial \theta} \\ \dfrac{1}{r}\dfrac{\partial u_i}{\partial \theta} + \dfrac{\partial v_i}{\partial r} - \dfrac{v_i}{r} \end{Bmatrix}, \quad \boldsymbol{\varepsilon}_{\mathrm{outp},i} = \begin{Bmatrix} \dfrac{\partial^2 w_i}{\partial r^2} \\ -\dfrac{1}{r}\left(\dfrac{\partial w_i}{\partial r} + \dfrac{1}{r}\dfrac{\partial^2 w_i}{\partial \theta^2}\right) \\ 2\left(\dfrac{1}{r^2}\dfrac{\partial w_i}{\partial \theta} - \dfrac{1}{r}\dfrac{\partial^2 w_i}{\partial \theta \partial r}\right) \end{Bmatrix}. \tag{17}$$

Matrix **D** is used to represent the element elastic properties as functions of the disc thickness and material characteristics; it can be split into two separate terms, too. Both can be computed under the assumption that the sections perpendicular to the radial directions remain plane after deformation and the effect of shear deformation is negligible:

$$\mathbf{D}_{\mathrm{inp}} = e_{\mathrm{inp}}\mathbf{d}, \quad \mathbf{D}_{\mathrm{outp}} = e_{\mathrm{outp}}\mathbf{d}, \tag{18}$$

where

$$e_{\mathrm{inp}} = Eh/(1-\upsilon^2), \quad e_{\mathrm{outp}} = Eh^3/12(1-\upsilon^2), \tag{19}$$

account for the in-plane and out-of-plane elastic behavior, E is Young's modulus, and

$$\mathbf{d} = \begin{bmatrix} 1 & \upsilon & 0 \\ \upsilon & 1 & 0 \\ 0 & 0 & (1-\upsilon)/2 \end{bmatrix}. \tag{20}$$

By substituting the discretized displacement equations and shape functions into Eq. (15), the elastic potential energy can be expressed as

$$U_{e\mathrm{inp},i} = \tfrac{1}{2}(\mathbf{q}_{ux}^{\mathrm{T}}\mathbf{k}_{uu,i}\mathbf{q}_{ux} + \mathbf{q}_{uy}^{\mathrm{T}}\mathbf{k}_{uu,i}\mathbf{q}_{uy} + \mathbf{q}_{vx}^{\mathrm{T}}\mathbf{k}_{vv,i}\mathbf{q}_{vx} + \mathbf{q}_{vy}^{\mathrm{T}}\mathbf{k}_{vv,i}\mathbf{q}_{vy} + \mathbf{q}_{ux}^{\mathrm{T}}\mathbf{k}_{uv,i}\mathbf{q}_{vx} + \mathbf{q}_{uy}^{\mathrm{T}}\mathbf{k}_{uv,i}\mathbf{q}_{vy}),$$

$$U_{e\mathrm{outp},i} = \tfrac{1}{2}(\mathbf{q}_{wx}^{\mathrm{T}}\mathbf{k}_{ww,i}\mathbf{q}_{wx} + \mathbf{q}_{wy}^{\mathrm{T}}\mathbf{k}_{ww,i}\mathbf{q}_{wy}), \tag{21}$$

where

$$\mathbf{k}_{uu,i} = \pi\int_{r_i}^{r_0} \frac{e_{\mathrm{inp}}}{2r^2}\{[2+i^2(1-\upsilon)]\mathbf{n}_u^{\mathrm{T}}\mathbf{n}_u + 2\upsilon r[\mathbf{n}_u^{\mathrm{T}}\mathbf{n}_u' + (\mathbf{n}_u')^{\mathrm{T}}\mathbf{n}_u] + 2r^2(\mathbf{n}_u')^{\mathrm{T}}\mathbf{n}_u'\}r\,\mathrm{d}r,$$

$$\mathbf{k}_{vv,i} = \pi\int_{r_i}^{r_0} \frac{e_{\mathrm{inp}}}{2r^2}\{[2i^2+(1-\upsilon)]\mathbf{n}_u^{\mathrm{T}}\mathbf{n}_u - r(1-\upsilon)[\mathbf{n}_u^{\mathrm{T}}\mathbf{n}_u' + (\mathbf{n}_u')^{\mathrm{T}}\mathbf{n}_u] + r^2(1-\upsilon)(\mathbf{n}_u')^{\mathrm{T}}\mathbf{n}_u'\}r\,\mathrm{d}r,$$

$$\mathbf{k}_{uv,i} = \mathrm{i}\pi\int_{r_i}^{r_0} \frac{e_{\mathrm{inp}}}{2r^2}[(3-\upsilon)\mathbf{n}_u^{\mathrm{T}}\mathbf{n}_u - r(1-3\upsilon)(\mathbf{n}_u')^{\mathrm{T}}\mathbf{n}_u']r\,\mathrm{d}r,$$

$$\begin{aligned}\mathbf{k}_{ww,i} = \pi\int_{r_i}^{r_0} \frac{e_{\mathrm{outp}}}{r^4}\{&[i^4+2i^2(1-\upsilon)]\mathbf{n}_w^{\mathrm{T}}\mathbf{n}_w - r[i^2+2i^2(1-\upsilon)][\mathbf{n}_w^{\mathrm{T}}\mathbf{n}_w' + (\mathbf{n}_w')^{\mathrm{T}}\mathbf{n}_w] \\ &+ r^2[1+2i^2(1-\upsilon)](\mathbf{n}_w')^{\mathrm{T}}\mathbf{n}_w' - \upsilon i^2 r^2[\mathbf{n}_w^{\mathrm{T}}\mathbf{n}_w'' + (\mathbf{n}_w'')^{\mathrm{T}}\mathbf{n}_w] - \upsilon r^3[(\mathbf{n}_w')^{\mathrm{T}}\mathbf{n}_w'' + (\mathbf{n}_w'')^{\mathrm{T}}\mathbf{n}_w'] + r^4(\mathbf{n}_w'')^{\mathrm{T}}\mathbf{n}_w''\}r\,\mathrm{d}r.\end{aligned} \tag{22}$$

The geometric potential energy $U_{g,i}$ is generated by the effect of centrifugal stiffening and thermal stresses in the disc. The restoring force due to centrifugal and thermal stresses is very important if the disc is like a membrane, i.e. has a low bending stiffness. This contribution can be expressed in the form

$$U_{g,i} = \frac{1}{2}\int_{r_i}^{r_0}\int_0^{2\pi}\left[\sigma_r\left(\frac{\partial w_i}{\partial r}\right)^2 + \sigma_c\left(\frac{1}{r}\frac{\partial w_i}{\partial \theta}\right)^2 + \sigma_r\left(\frac{\partial v_i}{\partial r}\right)^2 + \sigma_c\left(\frac{1}{r}\frac{\partial u_i}{\partial \theta}\right)^2\right]rh\,\mathrm{d}r\,\mathrm{d}\theta. \tag{23}$$

The radial and circumferential stresses σ_r and σ_c can be evaluated by using, for example, the Manson method [20]. A decoupling similar to the kinetic and elastic energy occurs between in-plane and out-of-plane degrees of freedom and the potential energy of i th-order harmonics can be written as

$$U_{g,i} = U_{g\mathrm{inp},i} + U_{g\mathrm{outp},i}. \tag{24}$$

Integrating the equations, the geometric potential energy is obtained:

$$U_{g\mathrm{inp},i}=\tfrac{1}{2}(\mathbf{q}_{ux}^{\mathrm{T}}\mathbf{k}_{gu,i}\mathbf{q}_{ux}+\mathbf{q}_{uy}^{\mathrm{T}}\mathbf{k}_{gu,i}\mathbf{q}_{uy}+\mathbf{q}_{vx}^{\mathrm{T}}\mathbf{k}_{gv,i}\mathbf{q}_{vx}+\mathbf{q}_{vy}^{\mathrm{T}}\mathbf{k}_{gv,i}\mathbf{q}_{vy}),$$

$$U_{g\mathrm{outp},i}=\tfrac{1}{2}(\mathbf{q}_{wx}^{\mathrm{T}}\mathbf{k}_{gwc,i}\mathbf{q}_{wx}+\mathbf{q}_{wy}^{\mathrm{T}}\mathbf{k}_{gwc,i}\mathbf{q}_{wy}+\mathbf{q}_{wx}^{\mathrm{T}}\mathbf{k}_{gwr,i}\mathbf{q}_{wx}+\mathbf{q}_{wy}^{\mathrm{T}}\mathbf{k}_{gwr,i}\mathbf{q}_{wy}). \tag{25}$$

The stiffness matrices are given by the integrals of the shape functions

$$\mathbf{k}_{gv,i}=\pi\int_{r_i}^{r_0}\sigma_r hr(\mathbf{n}'_v)^{\mathrm{T}}\mathbf{n}'_v\,\mathrm{d}r,\quad \mathbf{k}_{gu,i}=i^2\pi\int_{r_i}^{r_0}\frac{\sigma_c h}{r}\mathbf{n}_u^{\mathrm{T}}\mathbf{n}_u\,\mathrm{d}r,$$

$$\mathbf{k}_{gwr,i}=\pi\int_{r_i}^{r_0}\sigma_r hr(\mathbf{n}'_w)^{\mathrm{T}}\mathbf{n}'_w\,\mathrm{d}r,\quad \mathbf{k}_{gwc,i}=i^2\pi\int_{r_i}^{r_0}\frac{\sigma_c h}{r}\mathbf{n}_w^{\mathrm{T}}\mathbf{n}_w\,\mathrm{d}r. \tag{26}$$

2.3.3. Element matrices

Second and higher order harmonics are uncoupled from the flexural behavior of rotor. If no external force acts on the element, the equations of motion for the second and higher order harmonics have the same form as in Ref. [8]:

$$\mathbf{M}_{\mathrm{inp},i}\ddot{\mathbf{Q}}_{\mathrm{inp},i}-\mathrm{i}\omega\mathbf{G}_{\mathrm{inp},i}\dot{\mathbf{Q}}_{\mathrm{inp},i}+(\mathbf{K}_{\mathrm{inp},i}+\omega^2\mathbf{K}_{\omega\mathrm{inp},i}-\omega^2\mathbf{M}_{ni\mathrm{inp},i})\mathbf{Q}_{\mathrm{inp},i}=\mathbf{0},$$

$$\mathbf{M}_{\mathrm{outp},i}\ddot{\mathbf{Q}}_{\mathrm{outp},i}-\mathrm{i}\omega\mathbf{G}_{\mathrm{outp},i}\dot{\mathbf{Q}}_{\mathrm{outp},i}+(\mathbf{K}_{\mathrm{outp},i}+\omega^2\mathbf{K}_{\omega\mathrm{outp},i}-\omega^2\mathbf{M}_{ni\mathrm{outp},i})\mathbf{Q}_{\mathrm{outp},i}=\mathbf{0}. \tag{27}$$

The in-plane and out-of-plane motions can be assembled in vectors as

$$\mathbf{Q}_{\mathrm{inp},i}=\left\{\begin{matrix}\mathbf{q}_{ux}+\mathrm{i}\mathbf{q}_{uy}\\ \mathbf{q}_{vx}+\mathrm{i}\mathbf{q}_{vy}\end{matrix}\right\}_{(4\times1)},\quad \mathbf{Q}_{\mathrm{outp},i}=\{\mathbf{q}_{wx}+\mathrm{i}\mathbf{q}_{wy}\}_{(4\times1)}. \tag{28}$$

The element mass, gyroscopic, centrifugal stiffening, thermal gradients and stiffness matrices are obtained from the element kinetic and potential energies through Lagrange's equations

$$\mathbf{M}_{\mathrm{inp},i}=\begin{bmatrix}\mathbf{m}_{\mathrm{inp},i} & 0\\ 0 & \mathbf{m}_{\mathrm{inp},i}\end{bmatrix},\quad \mathbf{M}_{\mathrm{outp},i}=\mathbf{m}_{\mathrm{outp},i},$$

$$\mathbf{G}_{\mathrm{inp},i}=2\mathrm{i}\begin{bmatrix}\mathbf{m}_{\mathrm{inp},i} & -\mathbf{m}_{\mathrm{inp},i}\\ -\mathbf{m}_{\mathrm{inp},i} & \mathbf{m}_{\mathrm{inp},i}\end{bmatrix},\quad \mathbf{G}_{\mathrm{outp},i}=2\mathrm{i}\mathbf{m}_{\mathrm{outp},i},$$

$$\mathbf{M}_{ni\mathrm{inp},i}=\mathrm{i}^2\begin{bmatrix}\mathbf{m}_{\mathrm{inp},i} & -\mathbf{m}_{\mathrm{inp},i}\\ -\mathbf{m}_{\mathrm{inp},i} & \mathbf{m}_{\mathrm{inp},i}\end{bmatrix},\quad \mathbf{M}_{ni\mathrm{outp},i}=\mathrm{i}^2\mathbf{m}_{\mathrm{outp},i}. \tag{29}$$

The stresses in the radial and tangential directions can be computed from centrifugal and thermal loadings, the latter is independent of the rotational speed. Thus the stress field can be written as

$$\sigma_r=\sigma_{rT}+\omega^2\sigma_{r\omega},\quad \sigma_c=\sigma_{cT}+\omega^2\sigma_{c\omega},$$

where σ_r and σ_c are the stresses in radial and circumferential direction of the disc, $\sigma_{r\omega}$ and $\sigma_{c\omega}$ are the centrifugal stresses due to a unit rotational speed, $\omega=1$ rad/s, while σ_{rT} and σ_{cT} indicate the stress field due to the thermal gradients. In this case, the stiffness matrices can be split as

$$k_{g,i}=k_{gT,i}+\omega^2k_{g\omega,i}.$$

The stiffness matrices can be obtained by taking into account the arrangement of vector (28):

$$\mathbf{K}_{\mathrm{inp},i}=\begin{bmatrix}\mathbf{k}_{uu,i}+\mathbf{k}_{guT,i} & -\mathbf{k}_{uvT,i}\\ -\mathbf{k}_{uvT,i}^{\mathrm{T}} & \mathbf{k}_{vv,i}+\mathbf{k}_{gvT,i}\end{bmatrix},\quad \mathbf{K}_{\omega\mathrm{inp},i}=\begin{bmatrix}\mathbf{k}_{gu\omega,i} & 0\\ 0 & \mathbf{k}_{gv\omega,i}\end{bmatrix},$$

$$\mathbf{K}_{\mathrm{outp},i}=\mathbf{k}_{ww,i}+\mathbf{k}_{gwcT,i}+\mathbf{k}_{gwrT,i},\quad \mathbf{K}_{\omega\mathrm{outp},i}=\mathbf{k}_{gwc\omega,i}+\mathbf{k}_{gwr\omega,i}. \tag{30}$$

The elements are implemented with a numerical integration routine based on a four point Gauss procedure since the expressions of the matrix terms are difficult to achieve by analytical integrations.

2.4. Shaft–disc transition element

Beam and disc elements cannot be directly linked to the present annular disc element and the compatibility of the displacement at the disc–shaft interface must be insured. A suitable transition element has thus been developed which is provided with two nodes, the first located at the inner radius of the transition element (outer radius of the beam) describes the interface between the beam and the disc, and the second located at the outer radius of the element. The two nodes have 2 complex degrees of freedom and 4 complex degrees of freedom for flexural behavior, respectively.

The matrices for the shaft–disc transition element have been obtained from those described above for the disc element by just deleting all rows and columns linked with the degrees of freedom at node 1. This corresponds to constraining the displacements of the point at the inner radius of the element as a rigid body motion.

3. Second and higher order harmonics array of blades element

The main assumptions to analyze the array of blades are that all blades are equal, are aligned along the radial direction and their shear center coincides with the center of mass of each section. The number of blades must be 3 or larger, so that the assumption that the array is axisymmetric is satisfied [9]. Another assumption is that the blades are modeled as Euler–Bernoulli beams, i.e. that shear deformations and rotational inertia of the cross-sections can be neglected.

A typical cross-section of a blade perpendicular to the radial direction is shown in Fig. 3. G is the mass center of the cross-section while T is the shear center of it.

The array is modeled as a two-dimensional object, all its properties concentrated in the mid-plane of the blade, like for the disc element. The deformation of the array is referred to the same reference plane of the disc that is a plane perpendicular to the inflected deformation of the shaft passing through the disc–shaft attachment. The array exits this reference plane owing to its flexibility.

Let u_j, v_j, and w_j be, respectively, the radial, tangential and axial displacement components of a point P_j of a section of the jth blade taken at a radius r. $\mathbf{P}_j$ is the coordinate in an inertial reference of point P expressed as

$$(\overline{\mathbf{P}_j-\mathbf{O}}) = (\overline{\mathbf{C}-\mathbf{O}}) + \prod_{k=1}^{4} \mathbf{R}_k(\{r\ \ 0\ \ 0\}^{\mathrm{T}} + \{u_j\ \ v_j\ \ w_j\}^{\mathrm{T}}), \tag{31}$$

where $\mathbf{C}$ is the coordinate of the shaft–disc attachment point, $\mathbf{R}_k$ are the rotation matrices as a function of angle of the rigid body motion as reported in Ref. [9].

The second and higher order harmonics are uncoupled with the flexural behavior of the rotor as a whole while being important in the study of the local modes of the bladed disc. Rigid body motions can thus be neglected since they are uncoupled and do not enter the formulation of the present model. According to these indications, the deformation in the initial frame of point can be represented as the same form as Eq. (3).

3.1. Element shape functions

To define the shape functions approximating the deformations of the array of blades, the latter has been subdivided into annular elements. A non-dimensional radius χ has been defined in the same way as seen for the disc element. A, I_2 and I_3 are the area of the cross-section of each blade and its area moments of inertia about the principal inertia axis (u_2, u_3 in Fig. 3) of the cross-section. They are, together with angle ψ, linear functions of the non-dimensional radius χ. The displacements u_j, v_j, w_j are then approximated by means of a truncated Fourier's series in the angular coordinate θ_j:

$$u_j(\chi,\theta_j,z,t) = u_0 + \sum_{i=1}^{n} (u_{ic}\cos i\theta_j + u_{is}\sin i\theta_j),$$

$$v_j(\chi,\theta_j,z,t) = v_0 + \sum_{i=1}^{n} (v_{ic}\cos i\theta_j + v_{is}\sin i\theta_j),$$

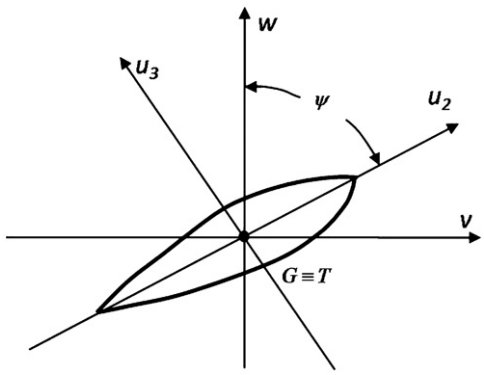

Fig. 3. Blade Cross-section; v, w: tangential and axial directions; u_2: axis of minimum principal moment of inertia; u_3: axis of maximum principal moment of inertia; ψ: pretwist angle of the blade.

$$w_j(\chi,\theta_j,z,t) = w_0 + \sum_{i=1}^{n}(w_{ic}\cos i\theta_j + w_{is}\sin i\theta_j). \tag{32}$$

The coefficient of the various harmonics displacement $u_{ic,s}$ and $v_{ic,s}$ refer to the in-plane displacement while $w_{ic,s}$ are related to the out-of-plane displacement.

The dynamic behavior of the zero- and first-order harmonics of array of blades element have already been studied in Ref. [9], and in this paper only the second and higher order harmonics are dealt with. Due to the orthogonality of trigonometric functions, all harmonics contributions are decoupled with each other, and the use of truncated Fourier's series expansion will not lead to any major approximations. Here the terms for each higher order harmonics are listed:

$$\begin{cases} u_{j,i}(\chi,\theta_j,t) = u_{ic}\cos i\theta_j + u_{is}\sin i\theta_j \\ v_{j,i}(\chi,\theta_j,t) = v_{ic}\cos i\theta_j + v_{is}\sin i\theta_j \\ w_{j,i}(\chi,\theta_j,t) = w_{ic}\cos i\theta_j + w_{is}\sin i\theta_j \end{cases} \quad \text{for } i \geq 2. \tag{33}$$

The use of shape functions to eliminate the displacement dependence on θ_j of the displacement field u, v, and w lead to the unknown functions in the same form as Eq. (5), which also can be approximated by shape functions written as Eq. (6).

The shape functions for the in-plane radial and out-of-plane deformations are the same as those used in the disc element, expressed in Eq. (7), while the in-plane circumferential deflection of the blade element is coupled with the out-of-plane deformation and can be expressed with the same cubic polynomial shape functions as the out-of-plane shape functions.

The generalized coordinates used to express the deflections of the array of blades coupled to the flexural behavior are

$$\mathbf{q}_{ux} = \{u_{x1}\ \ u_{x2}\}^{\mathrm{T}}, \quad \mathbf{q}_{uy} = \{u_{y1}\ \ u_{y2}\}^{\mathrm{T}},$$

$$\mathbf{q}_{vx} = -\{v_{x1}\ \ \beta_{wx1}\ \ v_{x2}\ \ \beta_{wx2}\}^{\mathrm{T}}, \quad \mathbf{q}_{vy} = \{v_{y1}\ \ \beta_{wy1}\ \ v_{y2}\ \ \beta_{wy2}\}^{\mathrm{T}},$$

$$\mathbf{q}_{wx} = \{w_{x1}\ \ \beta_{vx1}\ \ w_{x2}\ \ \beta_{wx2}\}^{\mathrm{T}}, \quad \mathbf{q}_{wy} = -\{w_{y1}\ \ \beta_{vy1}\ \ w_{y2}\ \ \beta_{vy2}\}^{\mathrm{T}}. \tag{34}$$

Two nodes are defined on the element, one at the inner radius of the element and the other at the outer radius. The total number of the real degrees of freedom of the element is 20; nodes 1 and 2 have 10 each. If complex coordinates are introduced into the equations of motion, 10 complex flexural degrees of freedom will be used.

3.2. Equations of motion of the element

The generalized coordinates used to approximate the displacements describe the deflections of the element from the rigid-body configuration. The equations of motion of the element have been written in the same way as already seen for the disc element.

3.2.1. Kinetic energy

The kinetic energy has been computed taking into account the contributions due to the rotational inertia of the array while the contributions of the rotational inertia the cross-section of a single blade is neglected when considering the deviations from the rigid-body configuration.

Let $\mathbf{P}_{j,i}$ denoting the displacement of the mass center of the jth blade at the radius r, relative to the inertial reference. The kinetic energy is

$$T_i = \frac{1}{2}\sum_{i=1}^{N}\int_{r_i}^{r_0} \rho A(r)\dot{\mathbf{P}}_{j,i}^{\mathrm{T}}\dot{\mathbf{P}}_{j,i}\,\mathrm{d}r, \tag{35}$$

where ρ is the density of the material of the blades and $A(r)$ is the cross-section of the blade at radius r.

In differentiating with respect to time, angle θ_j must be considered as a function of time. Owing to the orthogonality of the harmonic functions, a decoupling between the modes of the various orders occurs. The kinetic energy can be split into in-plane and out-of-plane contributions:

$$T_i = T_{\mathrm{inp},i} + T_{\mathrm{outp},i}. \tag{36}$$

The in-plane and out-of plane contributions to the kinetic energy can be expressed as functions of the shape function and element degrees of freedom as

$$\begin{aligned} T_{\mathrm{inp},i} = \tfrac{1}{2}[&\omega^2(\mathbf{q}_{ux}^{\mathrm{T}}\mathbf{m}_{\mathrm{inp1},i}\mathbf{q}_{ux} + \mathbf{q}_{uy}^{\mathrm{T}}\mathbf{m}_{\mathrm{inp1},i}\mathbf{q}_{uy} + \mathbf{q}_{vx}^{\mathrm{T}}\mathbf{m}_{\mathrm{inp2},i}\mathbf{q}_{vx} + \mathbf{q}_{vy}^{\mathrm{T}}\mathbf{m}_{\mathrm{inp2},i}\mathbf{q}_{vy} \\ &-2\mathbf{q}_{ux}^{\mathrm{T}}\mathbf{m}_{\mathrm{inp3},i}\mathbf{q}_{vx} - 2\mathbf{q}_{uy}^{\mathrm{T}}\mathbf{m}_{\mathrm{inp3},i}\mathbf{q}_{vy}) + \omega(\mathbf{q}_{uy}^{\mathrm{T}}\mathbf{m}_{\mathrm{inp1},i}\dot{\mathbf{q}}_{ux} - \mathbf{q}_{vy}^{\mathrm{T}}\mathbf{m}_{\mathrm{inp3},i}\dot{\mathbf{q}}_{ux} \\ &-\mathbf{q}_{ux}^{\mathrm{T}}\mathbf{m}_{\mathrm{inp1},i}\dot{\mathbf{q}}_{uy} + \mathbf{q}_{vx}^{\mathrm{T}}\mathbf{m}_{\mathrm{inp3},i}\dot{\mathbf{q}}_{uy} - \mathbf{q}_{uy}^{\mathrm{T}}\mathbf{m}_{\mathrm{inp3},i}\dot{\mathbf{q}}_{vx} + \mathbf{q}_{vy}^{\mathrm{T}}\mathbf{m}_{\mathrm{inp2},i}\dot{\mathbf{q}}_{vx} + \mathbf{q}_{ux}^{\mathrm{T}}\mathbf{m}_{\mathrm{inp3},i}\dot{\mathbf{q}}_{vy} \\ &-\mathbf{q}_{vx}^{\mathrm{T}}\mathbf{m}_{\mathrm{inp3},i}\dot{\mathbf{q}}_{vy}) + \dot{\mathbf{q}}_{ux}^{\mathrm{T}}\mathbf{m}_{\mathrm{inp1},i}\dot{\mathbf{q}}_{ux} + \dot{\mathbf{q}}_{uy}^{\mathrm{T}}\mathbf{m}_{\mathrm{inp1},i}\dot{\mathbf{q}}_{uy} + \dot{\mathbf{q}}_{vx}^{\mathrm{T}}\mathbf{m}_{\mathrm{inp2},i}\dot{\mathbf{q}}_{vx} + \dot{\mathbf{q}}_{vy}^{\mathrm{T}}\mathbf{m}_{\mathrm{inp2},i}\dot{\mathbf{q}}_{vy}], \\ T_{\mathrm{outp},i} = \tfrac{1}{2}[&\omega^2(\mathbf{q}_{wx}^{\mathrm{T}}\mathbf{m}_{\mathrm{outp},i}\mathbf{q}_{wx} + \mathbf{q}_{wy}^{\mathrm{T}}\mathbf{m}_{\mathrm{outp},i}\mathbf{q}_{wy}) + \omega(2\mathbf{q}_{wy}^{\mathrm{T}}\mathbf{m}_{\mathrm{outp},i}\dot{\mathbf{q}}_{wx} - 2\mathbf{q}_{wx}^{\mathrm{T}}\mathbf{m}_{\mathrm{outp},i}\dot{\mathbf{q}}_{wy}) \\ &+\dot{\mathbf{q}}_{wx}^{\mathrm{T}}\mathbf{m}_{\mathrm{outp},i}\dot{\mathbf{q}}_{wx} + \dot{\mathbf{q}}_{wy}^{\mathrm{T}}\mathbf{m}_{\mathrm{outp},i}\dot{\mathbf{q}}_{wy}]. \end{aligned} \tag{37}$$

Matrices $\mathbf{m}_{\mathrm{inp},i}$ and $\mathbf{m}_{\mathrm{outp},i}$ are given by the integrals:

$$\mathbf{m}_{\mathrm{inp1},i}=\frac{N}{2}\int_{r_i}^{r_0}\rho A\mathbf{n}_u^{\mathrm{T}}\mathbf{n}_u\,\mathrm{d}r,\quad \mathbf{m}_{\mathrm{inp2},i}=\frac{N}{2}\int_{r_i}^{r_0}\rho A\mathbf{n}_v^{\mathrm{T}}\mathbf{n}_v\,\mathrm{d}r,$$

$$\mathbf{m}_{\mathrm{inp3},i}=\frac{N}{2}\int_{r_i}^{r_0}\rho A\mathbf{n}_u^{\mathrm{T}}\mathbf{n}_v\,\mathrm{d}r,\quad \mathbf{m}_{\mathrm{outp},i}=\frac{N}{2}\int_{r_i}^{r_0}\rho A\mathbf{n}_w^{\mathrm{T}}\mathbf{n}_w\mathrm{d}r. \tag{38}$$

3.2.2. Potential energy

According to Ref. [9], contributions to the potential energy due both to the elastic strain–stress natural of the material ($U_{e,i}$) and to the geometric effect ($U_{g,i}$) have been considered:

$$U_i=U_{e,i}+U_{g,i}. \tag{39}$$

Shear deformation in the blade is neglected, since each single blade is modeled as an Euler–Bernoulli's beam. The elastic energy is thus related to the radial extension (axial deformation for the blade) and flexural deflections:

$$U_{e,i}=\frac{1}{2}\sum_{j=1}^{N}\int_{r_i}^{r_0}E\left[\frac{A}{\Delta r^2}(s'_{1,i})^2+\frac{1}{\Delta r^4}(I_2(s''_{2,i})^2+I_3(s''_{3,i})^2)\right]\mathrm{d}r. \tag{40}$$

The prime indicates the partial derivative related to the radial coordinates r and E is Young's modulus. The displacements s along the inertial axes are linked to the axial, tangential, radial directions by angle ψ

$$s_{1,i}=u_{j,i},$$

$$s_{2,i}=v_{j,i}\cos\psi+w_{j,i}\sin\psi,$$

$$s_{3,i}=w_{j,i}\cos\psi-v_{j,i}\sin\psi, \tag{41}$$

where angle ψ is a function of the radial coordinate only. Owing to the orthogonally of trigonometric functions, the in-plane and out-of-plane displacements are decoupled

$$(s'_{1,i})^2=(u'_{j,i})^{\mathrm{T}}u'_{j,i},$$

$$(s''_{2,i})^2=(v''_{j,i})^{\mathrm{T}}v''^2_{j,i}\cos^2\psi+(w''_{j,i})^{\mathrm{T}}w''_{j,i}\sin^2\psi,$$

$$(s''_{3,i})^2=(v''_{j,i})^{\mathrm{T}}v''_{j,i}\sin^2\psi+(w''_{j,i})^{\mathrm{T}}w''_{j,i}\cos^2\psi. \tag{42}$$

Prime indicates the partial derivative of the displacements u, v, w. The contributions to the elastic potential energy are expressed in terms of element generalized coordinates as

$$U_{e\mathrm{inp},i}=\tfrac{1}{2}(\mathbf{q}_{ux}^{\mathrm{T}}\mathbf{k}_{\mathrm{einp1},i}\mathbf{q}_{ux}+\mathbf{q}_{uy}^{\mathrm{T}}\mathbf{k}_{\mathrm{einp1},i}\mathbf{q}_{uy}+\mathbf{q}_{vx}^{\mathrm{T}}\mathbf{k}_{\mathrm{einp2},i}\mathbf{q}_{vx}+\mathbf{q}_{vy}^{\mathrm{T}}\mathbf{k}_{\mathrm{einp2},i}\mathbf{q}_{vy}),$$

$$U_{e\mathrm{outp},i}=\tfrac{1}{2}(\mathbf{q}_{wx}^{\mathrm{T}}\mathbf{k}_{\mathrm{eoutp},i}\mathbf{q}_{wx}+\mathbf{q}_{wy}^{\mathrm{T}}\mathbf{k}_{\mathrm{eoutp},i}\mathbf{q}_{wy}). \tag{43}$$

The stiffness matrices are obtained from the shape functions by the following integrals:

$$\mathbf{k}_{\mathrm{einp1},i}=\frac{N}{2\Delta r^2}\int_{r_i}^{r_0}EA(\mathbf{n}'_u)^{\mathrm{T}}\mathbf{n}'_u\,\mathrm{d}r,\quad \mathbf{k}_{\mathrm{einp2},i}=\frac{N}{2\Delta r^4}\int_{r_i}^{r_0}EI_w(\mathbf{n}''_v)^{\mathrm{T}}\mathbf{n}''_v\,\mathrm{d}r,$$

$$\mathbf{k}_{\mathrm{eoutp},i}=\frac{N}{2\Delta r^4}\int_{r_i}^{r_0}EI_v(\mathbf{n}''_w)^{\mathrm{T}}\mathbf{n}''_w\mathrm{d}r, \tag{44}$$

where I_v and I_w are the area moments of inertia of the cross-section in circumferential and axial direction v and w in Fig. 3.

The geometric potential energy is caused by the centrifugal forces $F_{r,i}$. Assuming that the blades are free to expand radially at their tips, the thermal effect do not induce any radial load along the axis of blades and force $F_{r,i}$ can be expressed as

$$F_{r,i}=\omega^2\int_r^{r_0}\rho Ar\,\mathrm{d}r=\omega^2P_{r\omega}(r). \tag{45}$$

The restoring force due to centrifugal stress is very important in the case of rotating pendulum. The geometric contribution to the potential energy can be expressed as

$$U_{g,i}=\frac{1}{2\Delta r^2}\sum_{i=1}^{N}\int_{r_i}^{r_0}F_{r,i}(r)[v'^2_{j,i}+w'^2_{j,i}]\,\mathrm{d}r. \tag{46}$$

The terms in the potential energy can be split into two independent contributions

$$U_{g,i}=U_{g\mathrm{inp},i}+U_{g\mathrm{outp},i}. \tag{47}$$

Substituting the shape functions and displacement equations into Eq. (45), the geometric potential energy is

$$U_{\mathrm{ginp},i} = \tfrac{1}{2}(\mathbf{q}_{vx}^{\mathrm{T}}\mathbf{k}_{\mathrm{ginp}\omega,i}\mathbf{q}_{vx} + \mathbf{q}_{vy}^{\mathrm{T}}\mathbf{k}_{\mathrm{ginp}\omega,i}\mathbf{q}_{vy}),$$

$$U_{\mathrm{goutp},i} = \tfrac{1}{2}(\mathbf{q}_{wx}^{\mathrm{T}}\mathbf{k}_{\mathrm{goutp}\omega,i}\mathbf{q}_{wx} + \mathbf{q}_{wy}^{\mathrm{T}}\mathbf{k}_{\mathrm{goutp}\omega,i}\mathbf{q}_{wy}). \tag{48}$$

The stiffness matrices are given by the integrals of the shape functions:

$$\mathbf{k}_{\mathrm{ginp}\omega,i} = \frac{N}{\Delta r^2}\int_{r_i}^{r_0} P_{r\omega}(\mathbf{n}'_v)^{\mathrm{T}}\mathbf{n}'_v \,\mathrm{d}r,$$

$$\mathbf{k}_{\mathrm{goutp}\omega,i} = \frac{N}{\Delta r^2}\int_{r_i}^{r_0} P_{r\omega}(\mathbf{n}'_w)^{\mathrm{T}}\mathbf{n}'_w \,\mathrm{d}r. \tag{49}$$

3.2.3. Element matrices

The equation of motion for the second and higher order harmonics of the array of blades element is the same as the equations describing the array of blades element in Ref. [9]. The in-plane and out-of-plane coordinates can be assembled in vectors as

$$\mathbf{Q}_{\mathrm{inp},i} = \left\{ \begin{matrix} \mathbf{q}_{ux} + \mathrm{i}\mathbf{q}_{uy} \\ \mathbf{q}_{vx} + \mathrm{i}\mathbf{q}_{vy} \end{matrix} \right\}_{(6\times 1)}, \quad \mathbf{Q}_{\mathrm{outp},i} = \{\mathbf{q}_{wx} + \mathrm{i}\mathbf{q}_{wy}\}_{(4\times 1)} \tag{50}$$

The element mass, gyroscopic, centrifugal and thermal stiffening and stiffness matrices are obtained by using Lagrange's equations

$$\mathbf{M}_{\mathrm{inp},i} = \begin{bmatrix} \mathbf{m}_{\mathrm{inp1},i} & 0 \\ 0 & \mathbf{m}_{\mathrm{inp2},i} \end{bmatrix}, \quad \mathbf{M}_{\mathrm{outp},i} = \mathbf{m}_{\mathrm{outp},i},$$

$$\mathbf{G}_{\mathrm{inp},i} = 2\mathrm{i}\begin{bmatrix} \mathbf{m}_{\mathrm{inp1},i} & -\mathbf{m}_{\mathrm{inp3},i} \\ -\mathbf{m}_{\mathrm{inp3},i} & \mathbf{m}_{\mathrm{inp2},i} \end{bmatrix}, \quad \mathbf{G}_{\mathrm{outp},i} = 2\mathrm{i}\mathbf{m}_{\mathrm{outp},i},$$

$$\mathbf{M}_{ni\mathrm{inp},i} = 2i^2\begin{bmatrix} \mathbf{m}_{\mathrm{inp1},i} & -\mathbf{m}_{\mathrm{inp3},i} \\ -\mathbf{m}_{\mathrm{inp3},i} & \mathbf{m}_{\mathrm{inp2},i} \end{bmatrix}, \quad \mathbf{M}_{ni\mathrm{outp},i} = i^2\mathbf{m}_{\mathrm{outp},i}. \tag{51}$$

The stresses in the radial and tangential directions can be computed from centrifugal and thermal loading. The stiffness matrices can be written as

$$\mathbf{K}_{\mathrm{inp},i} = \begin{bmatrix} \mathbf{k}_{e\mathrm{inp1},i} & 0 \\ 0 & \mathbf{k}_{e\mathrm{inp2},i} \end{bmatrix}, \quad \mathbf{K}_{\omega\mathrm{inp},i} = \begin{bmatrix} 0 & 0 \\ 0 & \mathbf{k}_{\mathrm{ginp}\omega,i} \end{bmatrix},$$

$$\mathbf{K}_{\mathrm{outp},i} = \mathbf{k}_{ww,i} + \mathbf{k}_{\mathrm{goutp},i}, \quad \mathbf{K}_{\omega\mathrm{outp},i} = \mathbf{k}_{\mathrm{goutp}\omega,i}. \tag{52}$$

The elements are implemented following the same numerical integration procedures as the disc element.

3.3. Disc–array of blades transition element

Even if the displacements within the array are very similar to those of the disc element, different kinds of shape functions are used for the tangential displacement fields (linear functions for the disc element; cubic functions for the array of blades) and thus a disc–blades transition element is needed. Two suitable transition elements should then be developed to insure the compatibility of the displacement fields at the shaft–array of blades (if the blades are connected directly to the shaft) and the disc–array of blades (if a disc is interposed between the shaft and the blades) interface. Due to the fact that the blades are seldom connected to the shaft directly, only the disc–array of blades transition element has been developed.

The disc–array of blades transition element is provided with a node 1 contains 4 complex degrees of freedoms for the flexural behavior which located at the inner radius of the transition element describes the interface between the disc and array of blades, while a node 2 which has 5 complex degrees of freedom for flexural behavior located at the outer radius of the transition element. Their matrices have been obtained from those derived for the array of blades element by constraining the rotation about the tangential directions at node 1.

4. Examples

4.1. Rotating membrane

A rotating membrane is a very thin disc with negligible flexural stiffness which constitutes a good test case for verifying the mass, gyroscopic and centrifugal stiffening matrices of the element in out-of-plane modes. In an analytical point of view [2], the natural frequencies of the membrane are proportional to the spin speed, vanishing at standstill, and the constant of proportionality does not depend on the geometrical or material characteristics of the structure but only on the mode considered. To obtain a FEM model approximating a membrane, the thickness and Young's modulus should be set at a very low value.

The test has been performed using the following data: thickness: 1×10^{-7} m; outer diameter: 1 m; inner diameter: 0 m; Young's modulus: 1×10^{-5} N/m^2; Poisson's ratio: 0.3; density: 7800 kg/m^3. Two models, respectively with four and nine disc element and one transition element, have been built and each model has been studied by using both the whole set of generalized coordinates and performing Guyan reduction, which only consider the out-of-plane degrees of freedom as the master ones. The Campbell diagram is obtained by repeating the computations at three different values of the spin speed, namely 0, 0.5 and 1 Hz. The results are compared with the analytical results obtained by Southwell [2]. The second- and third-order harmonics of the disc element are compared with those obtained for 2 and 3 nodal diameters. The ratio ω/Ω for the second- and third-order harmonics are reported in Table 1.

From the table it follows that the present element performs quite well, proved that a sufficient number of elements are used. Comparing the results of the two models with 5 elements and 10 elements, it is clear that the accuracy of the numerical results increases by increasing the number of elements in the model: the numerical results tend to the analytical solution [2]. If Guyan reduction is used, the results are accurate for the lower order modes, while for higher order modes the error gets much bigger, which sometimes is unacceptable. The number of elements and of master degrees of freedom required depends obviously on the orders of the natural frequency to be computed.

Another model has also been built using ANSYS 11.0 code with the same geometric and material parameters in previously developed FEM and analytical model. Both the centrifugal stiffening (angular velocity inertia) and gyroscopic effect (Coriolis force) are considered in the ANSYS model. The membrane is meshed with 1078 4-node shell element, SHELL181. The Campbell diagram is obtained by repeating the computations at five different values of the spin speed, namely 0, 0.25, 0.5, 0.75 and 1 Hz. The results of the second- and third-order harmonics are compared in Fig. 4.

The figure shows that the natural frequencies of the flexural behavior at standstill are vanishingly small, the first natural frequency for the second-order harmonics, as an example, is 2.1×10^{-21} Hz at standstill (present FEM model) and 5.7×10^{-6} Hz (ANSYS model). The natural frequencies increase linearly with speed according to the Campbell diagram, which is predicted by the theory. But the present FEM model matches very well the analytical result as already demonstrated in Table 1, while the ANSYS model under-estimates the whirl frequencies of not only the forward but also the backward mode, and the errors increase with the increasing speed, which indicates that compared to the analytical results and the finite element model, the conventional FEM codes yield poor results when gyroscopic terms are accounted for. Furthermore, the present FEM model requires a much smaller number of element than the ANSYS model (10 VS 1078), while providing a much better accuracy.

4.2. Constant thickness pierced non-rotating disc

Consider a constant thickness steel disc with the following geometrical and material data: thickness 5.94 mm; outer diameter 1220 mm; inner diameter 76.2 mm; Young's modulus 2.1×10^{11} N/m^2; Poisson's ratio 0.3 and density

Table 1
Ratio ω/Ω, for the first three backward and forward whirl frequencies for the second- and third-order harmonics.

	5 el.,. No red.	5 el.,. Gu.red.	10 el.,. No red.	10 el.,. Gu.red.	Ref.	Min error (%)	Max error (%)
Second-order harmonic disc							
1FWD	3.5322	3.5339	3.5328	3.5329	3.533	0.0057	0.0255
2FWD	4.9914	4.5022	4.9921	4.9988	4.992	0.0020	0.9811
3FWD	6.3421	6.4655	6.3422	6.4217	6.342	0.0032	1.9473
1BWD	0.4677	0.4695	0.4669	0.4672	0.467	0.0214	0.5353
2BWD	−0.9926	−0.9992	−0.9927	−0.9988	−0.992	0.0706	0.7258
3BWD	−2.3433	−2.3651	−2.3416	−2.3431	−2.342	0.0171	0.9863
Third-order harmonic disc							
1FWD	5.0127	5.0115	5.0133	5.0121	5.013	0.0060	0.0299
2FWD	6.5075	6.5094	6.5073	6.5086	6.507	0.0046	0.0369
3FWD	7.8862	7.9523	7.8857	7.9229	7.884	0.0216	0.8663
1BWD	0.9889	0.9854	0.9986	0.9767	0.998	0.0601	1.2625
2BWD	−0.5076	−0.5095	−0.5071	−0.5088	−0.507	0.0197	0.4931
3BWD	−1.8861	−1.9522	−1.8847	−1.8972	−1.884	0.0372	3.6200

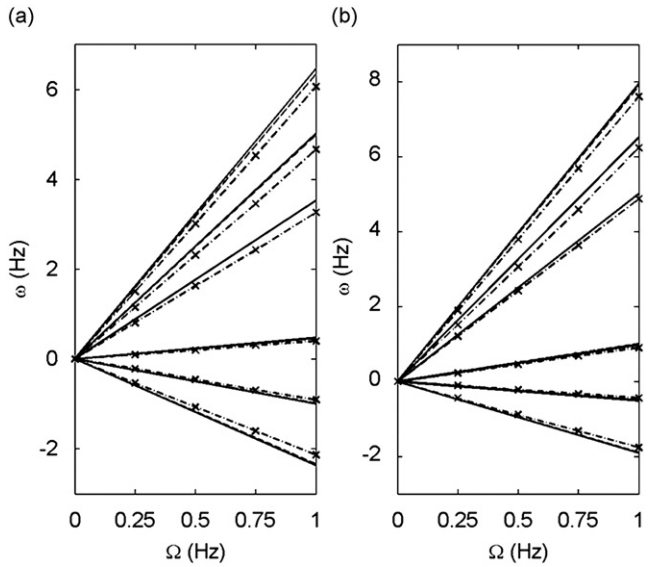

Fig. 4. Comparison of the Campbell diagrams of the second- and third-order harmonics with analytical, FEM and ANSYS model; (a) second-order harmonics; (b) third-order harmonics; solid line: analytical results; dashed line: FEM results; dash dot line with $\times$: ANSYS results.

Table 2
Comparison between the first three natural frequencies for the second- and third-order harmonics, $\omega = 0$.

Freq. (Hz)	No red.	Guyan red.	ANSYS	Min error (%)	Max error (%)
Second-order harmonic disc					
#1 mode	21.810	21.886	21.765	0.2068	0.5559
#2 mode	143.483	143.597	143.164	0.2228	0.3025
#3 mode	346.984	347.189	345.712	0.3679	0.4272
Third-order harmonic disc					
#1 mode	49.632	49.699	49.597	0.0706	0.2057
#2 mode	211.687	211.906	211.466	0.1045	0.2081
#3 mode	448.254	448.775	447.365	0.1987	0.3152

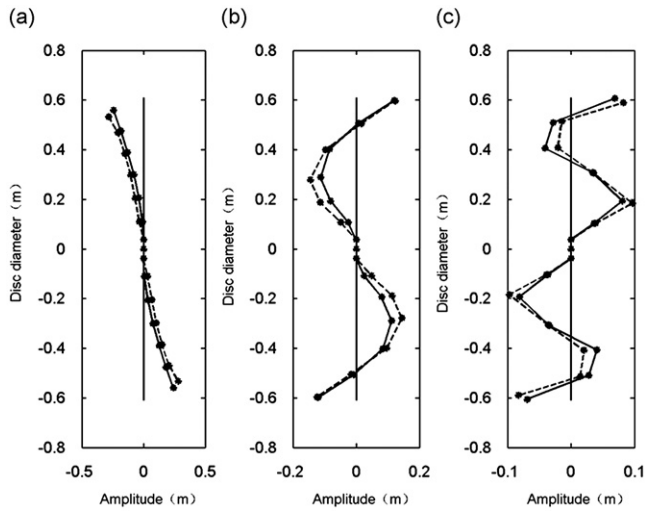

Fig. 5. First three order modes of second-order harmonics for ANSYS and DYNROT models, $\omega = 0$; (a) first-order mode; (b) second-order mode; (c) third-order mode; solid line: undeformed disc; solid line with *: mode of DYNROT model; dash line with *: mode of ANSYS model.

7800 kg/m^3. As no analytical solutions are available, the comparison is made by using the results obtained using the ANSYS 11.0 code, with 1642 4-node shell elements, SHELL181. The first 30 frequencies for null angular speed are obtained by using a Block Lanczos technique. The present finite element model is built using one shaft–disc transition element and five disc elements. The solution is performed both by resorting and not resorting to Guyan reduction, which consider the out-of-plane degrees of freedom as the master ones. Only the first three natural frequencies for the second- and third-order harmonics are computed which are reported in Table 2. The first three mode shapes for the second-order harmonics disc element and ANSYS model are plotted using non-dimensional deformation in Fig. 5.

From all the data above it follows that at null angular speed whatever the reduction method is used or not, not only the frequencies but also the modes for the higher order harmonics in a case of constant thickness pierced non-rotating disc fits very well with the maximum error at about 0.5 percent.

4.3. Variable thickness pierced non-rotating disc

Now consider a steel disc whose thickness is variable in radial direction. The cross-section of the disc is illustrated in Fig. 6. Geometrical and material data are: outer diameter 640 mm; inner diameter 40 mm; Young's modulus 2.1×10^{11} N/m^2; Poisson's ratio 0.3 and density 7800 kg/m^3. A FEM model with one transition element and nine disc elements is built, and a comparison model has been set up using ANSYS 11.0 with 4684 eight node three-dimensional structural solid element, SOLID45. The first three frequencies at null angular speed of the second-order harmonics are compared in Table 3. The mode shapes are plotted using non-dimensional deformation in Fig. 7.

The precision obtained is remarkable. For the lowest three frequencies of the second-order harmonics element the maximum error is about 1 percent, which means for the disc if the thickness in radial direction is changed, the higher order harmonics element is also perfectly suitable. But if the thickness in radial direction is nonlinear, it is clear that more disc elements which are shorter in radial direction must be used to approximate the thickness changing. These tests on non-rotating systems show that the stiffness matrix, not tested in the example on the membrane, is essentially correct (or at least, yields the same results as commercial FEM codes).

4.4. Variable thickness pierced rotating disc

Consider the same steel disc studied in Example 4.3, but now taking into account rotation, with a speed range between 0 and 100 Hz. The mathematical model is the same as seen already, but here a further model in which the gyroscopic terms are neglected is studied. The results are compared with ANSYS 11.0 in Fig. 8. The frequencies computed using DYNROT and ANSYS codes are in accordance at standstill. When considering rotation, DYNROT model still agrees with ANSYS model if the gyroscopic effect is neglected. This means that in both models only centrifugal stiffening is taken into consideration.

If all the contributions in DYNROT model are accounted for, ANSYS code under-estimates the whirl frequencies of both forward and backward mode and these errors increase with increasing speed. It proves that the conventional FEM codes make worse approximation and consequently reach worse accuracy than the present one when the gyroscopic effect is accounted for, even though the ANSYS model is meshed with much more elements than the present DYNROT model (4684 Vs 10).

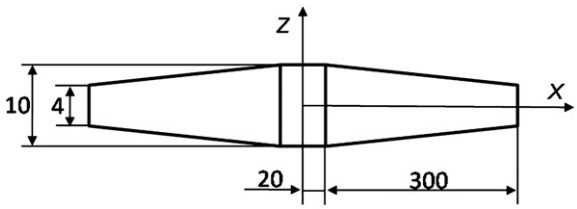

Fig. 6. Cross-section of the pierced non-rotating disc (unit: mm).

Table 3
Comparison between the first three nature frequencies for second-order harmonics, $\omega=0$.

Freq. (Hz)	10 element no reduction	ANSYS 11.0	Error (%)
Second-order harmonic disc			
#1 mode	221.0498	218.52	1.14
#2 mode	1279.8227	1271	0.61
#3 mode	3094.0415	3098	0.13

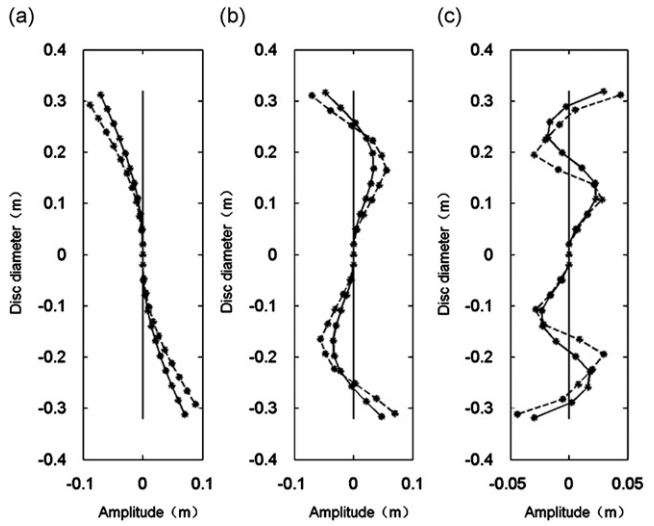

Fig. 7. First three order mode of second-order harmonics for ANSYS and DYNROT models, $\omega = 0$; (a) first-order mode; (b) second-order mode; (c) third-order mode; solid line: undeformed disc; solid line with $*$ mode of DYNROT model; dash line with $*$: mode of ANSYS model.

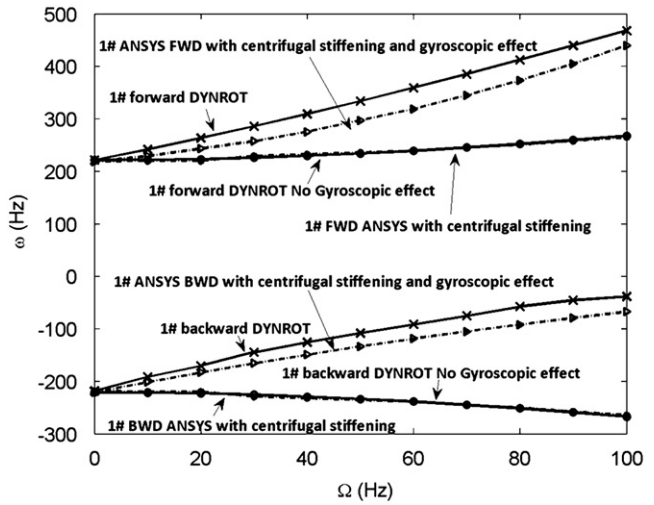

Fig. 8. First forward and backward frequencies as functions of the speed for the plate in DYNROT and ANSYS model.

4.5. Rotating pendulum

A rotating pendulum is a limit case for testing the inertial and centrifugal stiffening matrices of the present array of blades element. The natural frequencies of the rotating pendulum are related to the spinning speed by the relationships

$$\lambda_1 = \omega\sqrt{1+r/l}, \quad \lambda_2 = \omega\sqrt{r/l}, \tag{53}$$

where l is the length of the pendulum and r is the radius of the disc.

The disc at which the pendulum is attached is modeled using two beam elements for the shaft constrained at both ends by rigid supports, one shaft–disc transition element, one disc element, and all these elements being very stiff. A disc–array of blades transition element and nine array of blades elements are added to model the pendulum. All geometrical and material data come from Ref. [9]. The computation is performed at a speed 100 rad/s, at which the natural frequencies of the in-plane and out-of-plane oscillations of the pendulum computed using Eq. (53) are 100 and 141.41 rad/s, respectively. The results for the second-order harmonic components, seen as the flexural oscillations of the row corresponding to the in-plane and out-of-plane oscillations of all pendulums, have been reported in Table 4. Each oscillation mode generates two flexural modes, which are backward and forward, respectively.

Table 4
Rotating pendulum, flexural natural frequencies compared through current model and theory, $\omega = 100$ rad/s.

		DYNROT model	Analytical result	Error (%)
Second-order harmonic array of blades				
#1 in-plane (rad/s)	FWD	201.77	200	0.88
	BWD	0.177	0	–
#1 out-of-plane (rad/s)	FWD	243.19	241.421	0.73
	BWD	−4.319	−4.142	4.09

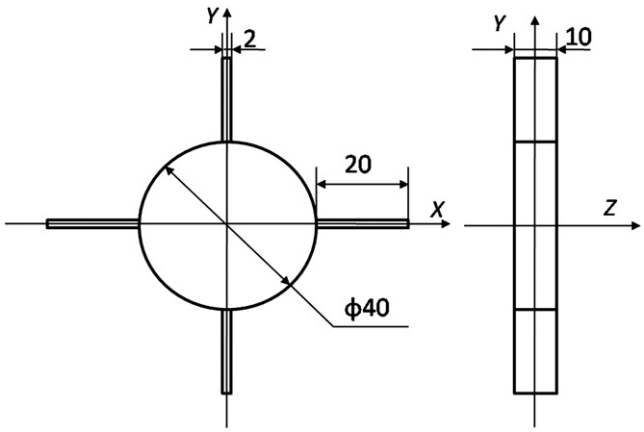

Fig. 9. Geometric structure of the model built both in ANSYS and DYNROT (unit: mm).

Table 5
Disc with array of blades: comparison between the first three natural frequencies for the second-order harmonics, $\omega = 0$.

Freq. (Hz)	No red.	Guyan red.	ANSYS	Min error (%)	Max error (%)
Second-order harmonic array of blades					
#1 mode	128.321	129.007	128.001	0.2500	0.7859
#2 mode	453.282	457.186	451.558	0.3818	1.2464
#3 mode	804.228	796.218	813.22	1.1057	2.0907

The natural frequencies are also computed at other values of the spin speed, showing a linear dependence as predicted by the theory. The present model yields results which are close to the correct ones.

4.6. *Shaft with flexible disc and blades*

A finite element model with a shaft and a flexible disc and four prismatic blades are considered to verify the behavior at standstill. A model with a cylinder and four beams is also set up using ANSYS 11.0 which is meshed with 4054 eight node three-dimensional structural solid element, SOLID45, to compare the results. The geometric configuration of the rotor structure is given in Fig. 9. The material parameters are: density 7800 kg/m^3, Poisson's ratio 0.3, Young's modulus 2.1×10^{11} N/m^2.

This model is only used to verify the modes related to second and higher order harmonics of the array of blades. The DYNROT model is made of two beam elements for the shaft, whose ends are constraint by rigid supports, one shaft–disc transition element, one disc element, a disc–array of blades transition element and nine array of blades elements. The computation is performed both by using all generalized coordinates and using Guyan reduction, which determines the out-of-plane degrees of freedoms as the master degrees of freedom. Only the first three natural frequencies for the second-order harmonics are computed and compared with the results reported in Table 5. The first three mode shapes for the second-order harmonics element and ANSYS model and the compare of mode shape using non-dimensional deformation of each blade are plotted in Fig. 10.

It indicates that whatever the reduction method is used or not, the frequencies for the second and higher order harmonics in a case of shaft with flexible disc and prismatic blades fit very well with a maximum error of no more than

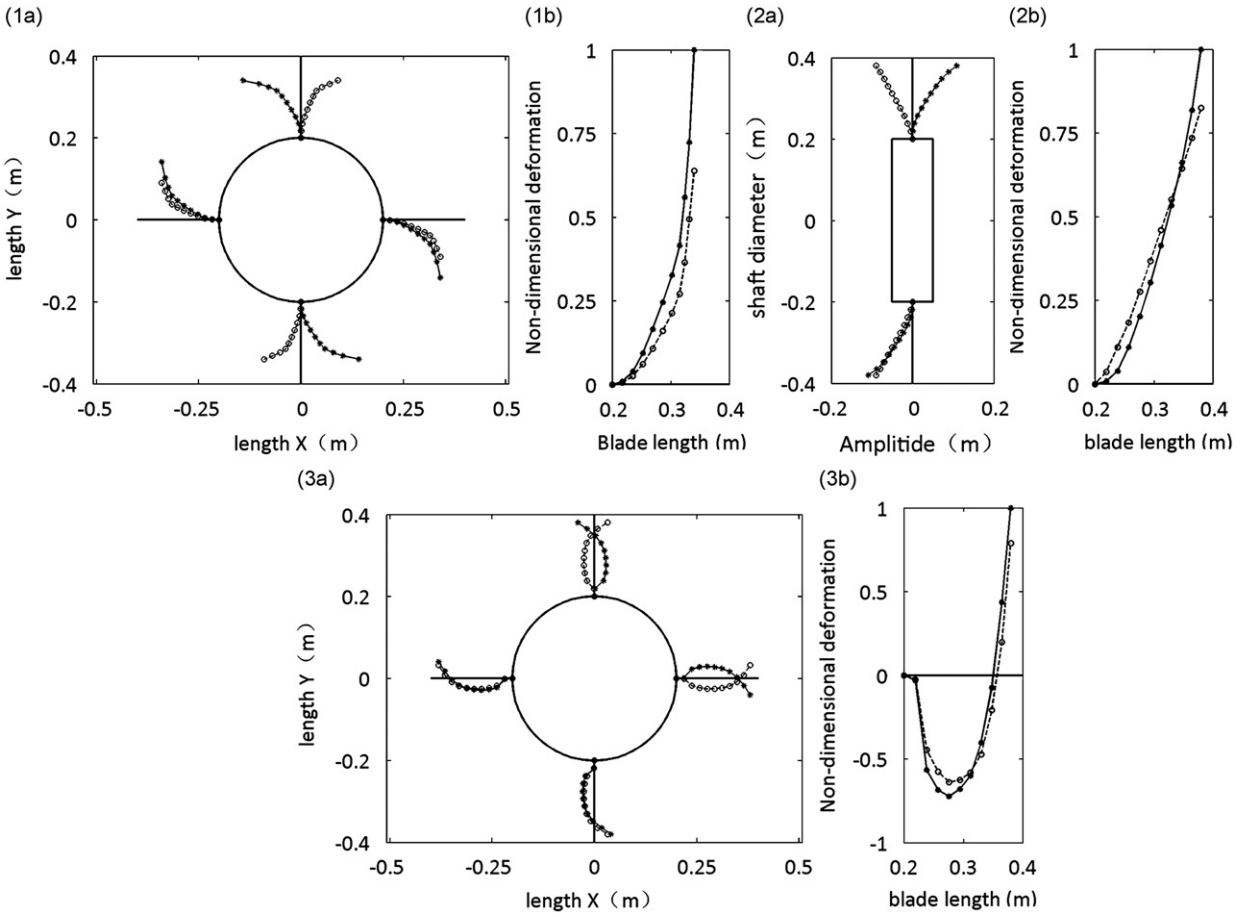

Fig. 10. First three order modes of second-order harmonics for ANSYS and DYNROT models, $\omega = 0$; (1a), (2a), (3a): first-, second- and third-order mode of bladed disc of second-order harmonics; (1b), (2b), (3b) non-dimensional deformation of a single blade in radial direction of first-, second- and third-order mode; solid line with $\times$: undeformed blades; solid line with $\circ$: blade mode of DYNROT model; dash line with $\circ$: blade mode of ANSYS model.

2 percent. Also the mode shapes for higher order harmonics of DYNROT model are in good agreement with that of ANSYS though some of the blades have 180° phase difference. But as the disc has been completely constrained, the dynamics of each blade is decoupled from the others, which means the phase difference of some blades in DYNROT model relative to ANSYS modes is not relevant.

5. Conclusions

Two finite elements aimed at modeling discs and arrays of blades for the studying of their flexural behavior have been developed. Both the displacement field within the disc element and array of blades are approximated by trigonometrical expansion along the tangential direction and a polynomial expansion along the radius. Only the second and higher order harmonics have been taken into account as they are uncoupled from the dynamic behavior of the rotor.

The formulation for both elements have been obtained using complex coordinates following a Lagrangian approach which accounts for gyroscopic effects and stress stiffening. The elements have been implemented in the existing FEM code DYNROT. For disc element a constant stress contribution has been considered, for example due to the thermal stresses, and assumed as a part proportional to the square of the spin speed. However, for blade array elements, the constant stress contribution has not been considered as the blades are assumed to be unconstrained in the radial direction at their tip and thermal gradient is not considered in array of blades element.

Since the modes of the disc here studied are uncoupled with the modes of the shaft, the disc element has two nodes, one at the inner radius of the element and the other at the outer radius. Also the array of blades element is provided with two nodes, being located at the element inner and outer radii. Two transition elements have been developed to connect the disc element with beam element used to model the shaft and array of blades element with disc element, respectively. It is

assumed that the discs are attached to the outer radius of the shaft and blades are clamped to the disc at the inner radius of the array.

A number of tests have been carried out to verify the accuracy of the two elements. For the disc element, a membrane has first been studied to compare the analytical results with the natural frequencies obtained by the current disc element model and ANSYS code.

A very interesting result is that, while the present element formulation yields results that coincide with the analytical solutions, the results obtained through ANSYS are different, and in particular yield a value of the natural frequencies that is lower than the analytical one. Then several cases are used to compare the natural frequencies considering the different geometric structure of discs modeled using the present disc element and a commercial FEM code, ANSYS 11.0. The results show the disc element performs with a good accuracy, even when using a small number of degrees of freedom.

Again, when the Coriolis terms are included the ANSYS model yields results that are different from the present ones while the results obtained neglecting Coriolis terms coincide. From the results obtained for the rotating membrane, apparently the formulation for the gyroscopic term in ANSYS yields a worse approximation than the present one.

For the array of blades element, both the analytical results obtained using a rotating pendulum and the numerical results achieved by rotating untwisted blades connected to a rigid disc and a rigid shaft have been compared to those given by the array of blades element, showing in both cases a good agreement. In addition, the present finite element model requires a smaller number of degrees of freedom than conventional FEM models, while still preserving its accuracy and, in some cases, yielding much more accurate results.

References

[1] S.G. Hutton, S. Chonan, B.F. Lehmann, Dynamic response of a guided circular saw, *Journal of Sound and Vibration* 112 (1987) 527–539.
[2] H. Lamb, R.V. Southwell, The vibration of a spinning disk, *Proceeding of Loyal Society of London* 99 (1921) 272–280.
[3] J. Kirkhope, G.J. Wilson, Vibration of stress of the thin rotating disks using annular finite element, *Journal of Sound and Vibration* 44 (1976) 461–474.
[4] J. Mackerle, Finite element analysis of machine elements: a bibliography (1977–1997), *Engineering Computations* 16 (1999) 677–748.
[5] M. Sakata, K. Kimura, S.K. Park, Vibration of bladed flexible rotor due to gyroscopic moment, *Journal of Sound and Vibration* 131 (1989) 417–430.
[6] P.J. Magari, L.A. Shultz, V.R. Murthy, Dynamics of helicopter rotor blades, *Computer and Structure* 29 (1988) 763–782.
[7] G. Genta, On the stability of rotating blade arrays, *Journal of Sound and Vibration* 273 (2004) 805–836.
[8] G. Genta, A. Tonoli, A harmonic finite element for the analysis of flexural, torsional and axial rotordynamic behavior of discs, *Journal of Sound and Vibration* 196 (1996) 19–43.
[9] G. Genta, A. Tonoli, A harmonic finite element for the analysis of flexural, torsional and axial rotordynamic behavior of blade arrays, *Journal of Sound and Vibration* 207 (1997) 693–720.
[10] J. H Choi, I. Lee, Finite element analysis of transient thermo-elastic behaviors in disk brakes, *Wear* 257 (2004) 47–58.
[11] A. Leissa, Vibration aspects of rotating turbo machinery blades, *Applied Mechanics Review* 34 (1981) 629–635.
[12] S.B. Chun, C.W. Lee, Vibration of analysis of shaft-bladed disc system by using substructure synthesis and assumed mode method, *Journal of Sound and Vibration* 189 (1996) 587–608.
[13] T. Tomioka, Y. Kobayashi, G. Yamada, Analysis of free vibration of rotating disc-blade coupled systems by using artificial springs and orthogonal polynomials, *Journal of Sound and Vibration* 191 (1996) 53–73.
[14] G.C. Ruzicka, D.H. Hodges, Application of the mixed finite-element method to rotor blade modal reduction, *Mathematical and Computer Modeling* 33 (2001) 1177–1202.
[15] J. Kang, Squeal analysis of gyroscopic disc brake system based on finite element method, *International Journal of Mechanical Sciences* 51 (2009) 284–294.
[16] S. Lim, Finite element analysis of flexural vibrations in hard disk drive spindle system, *Journal of Sound and Vibration* 233 (2000) 601–616.
[17] G. Genta, *Dynamics of Rotating System*, Springer, New York, 2007.
[18] G. Genta, *Vibration Dynamics and Control*, Springer, New York, 2009.
[19] G. Genta, C. Delprete, D. Bassini, DYNROT: a finite element code for rotordynamic analysis based on complex co-ordinates, *Engineering Computations* 13 (1996) 86–109.
[20] S.S. Manson, The determination of elastic stresses in gas turbine disks, NACA TN 1279, 1947.